Journal of Mines, Metals and Fuels, *71(12C) : 225-233; 2023. DOI: 10.18311/jmmf/2023/47299*

Print ISSN : 0022-2755

Journal of Mines, Metals and Fuels

Contents available at: *www.informaticsjournals.com/index.php/jmmf*

An Exploratory Analysis of MHD Non-Newtonian Nanomaterial Fluids Flow Across an Exponential Elongated Sheet

P. A. Dinesh[1*], R. Sumithra[2], C. V. Vinay[3], N. L. Ramesh[1], G. K. Kalavathi[4], N. J. Sahana[2], R. Gayithri[2], M. Pooja[2] and H. V. Vandana[2]

[1]Department of Mathematics, M. S. Ramaiah Institute of Technology, Bangalore - 560054, Karnataka, India; dineshdpa@msrit.edu, nlramesh@msrit.edu

[2]Department of Mathematics, Nrupathunga University, Bangalore - 560054, Karnataka, India; sumitradiya@yahoo.com, sahananj03@gmail.com, gayithrirgowda123@gmail.com, poojamaruthi18@gmail.com, vandanagowda668@gmail.com

[3]Department of Mathematics, JSS Academy of Technical Education, Bangalore - 560060, India; vinaycv@jssateb.ac.in

[4]Department of Mathematics, Malnad College of Engineering, Hassan - 573202, Karnataka,India; gkk@mcehassan.ac.in

Abstract

This paper aims to calculate the temperature, mass diffusion and flow characteristics of the boundary layer of Casson and Carreau fluids through an exponentially expanding surface where the normal flow of nanomaterials with magnetic properties is zero. In addition, the Buongiorno paradigm represents an even more plausible scenario in which passively controlled nanoparticles are considered at the surface. After that, an effective shooting method based on Runge-Kutta is applied to solve the modified equations. Plots are used to analyse the effects of viscous dispersion, radiant heat and the joule influence of the chosen flow control variables on the conventional profiles, including speed, temperature, and mass diffusion. A tabular representation of the numerical approach for the friction component and Nusselt number is provided. The Lorentz force significantly impacts Carreau fluid in contrast to Casson fluid.

Keywords: Carreau Fluid, Casson Fluid, Exponential Stretching Sheet, MHD

1.0 Introduction

The relationship between electromagnetic and magnetic characteristics is the subject of Magnetohydrodynamic (MHD) research. It is widely used in the production of pumps, flow yards, MHD power plants, ball bearings and other devices. The peculiar characteristics of nanomaterials are caused by the existence of zinc (Zn), Copper (Cu), Manganese (Mn), Iron (Fe), Titanium Dioxide (Ti) and other metallic nanoparticles. Many technical devices that maintain metal liquid and ionised flow in opposition to magnetic fields detect the MHD boundary layer. We refer to this kind of force as resistive force. The study of MHD boundary flows via a stretched surface has already been presented by several scholars[1–5]. This study examines the viscosity approach, such as the Carreau rheological model, from the generalised Newtonian fluids. The cohesiveness of the various polymeric solutions—poly ethylene oxide, 1% methylcellulose tylose and 0.3% hydroxyethyl-cellulose colourless solution—can be well characterised by the Carreau fluid's properties. Typically, the technique of

**Author for correspondence*

capillary electrophoresis uses those polymeric mixtures to improve the protein and DNA isolation[6–9].

There are several uses for investigating the properties of fluids that are not Newtonian in industries and engineering specifically the process of separating petroleum-based goods from petroleum. Another fluid that is regarded as unconventional is Casson fluid. Casson invented the Casson fluid in 1859. It makes the yielding stress visible. It behaves like a solid whenever shear stress is low yet acts like a liquid otherwise. Examples of Casson fluid include colour, tomato-based jam, honey, strong juice from fruits and soup. Pramanik[10] illustrated the heat transmission flow across a stretched sheet with electromagnetic radiation, noting that increasing Casson parameter values increase surface stress. Hayat *et al.*,[11] examined the MHD heat transfer Casson fluid past a stretched sheet amid a field of magnets. The convection movement of MHD towards an expanded sheet due to slip effects was covered by Sulochana and Sandeep[12]. They concluded that increasing the value of the magnetic field parameter diminishes skin friction and the Nusselt number.

Nadeem *et al.*,[13] investigated the MHD mass and heat transmission on the Casson liquid past a stretched surface. The computational solution for border layer MHD mass and heat transport across a curved sheet having the presence of a Casson fluid was given by Roopa *et al.*,[14] The impact of an electromagnetic field on the MHD flow pattern of Carreau fluids under convective boundaries was investigated by Khan *et al.*,[15]. The computational solution of the MHD Carreau fluid across a stretched surface having radiation impact was studied by Bhatti *et al*,.[16]. For MHD flows, the transfer of heat via convection was examined by the researchers[17–19]. The MHD mixed convection circulation of a micropolar medium over a stretched surface including viscous dispersion and Joule heating impacts was covered by Ahmed *et al.*,[20]. The effect of solar radiation upon MHD thermal flux across permeable pathways was examined and numerically resolved using a numerical approach by Sweeti *et al.*,[21] compressing movement of nanofluid across a stretched surface with magnetic field influences.

This article examined how thermophoresis and the Brownian moment influence MHD. Fluids having a magnetic field influence that are Carreau and Casson flow in the direction of a stretched surface. The alternate approaches for the Carreau and Casson instances were introduced by us. After being converted into a series of Ordinary Differential Equations (ODEs), the ensuing non-linear PDE was resolved by Runge-Kutta using the shooting approach. Tables and graphs are used to examine the impact of different variables on the flow, heat and mass diffusion as well as skin friction and Nusselt number.

2.0 Mathematical Formulation

Assume a continuous, incompressible, two-dimensional flow of Carreau and Casson streams in the direction of an exponentially expanding surface. The y-axis, on the other hand, is perpendicular to the outer layer and the x-axis is passed via an elastic sheet in the plane of flow. In the x-axis, the exponential sheet of expansion is assumed with velocity to elucidate at $y = 0$, where the exponential parameter is N and length is L. The current concept is thought to address the Casson flow and Carreau flow when $n = 1$ and when $\beta \to \infty$ Respectively. Brownian motion phenomena and thermophoresis are also taken into account. As seen in Figure 1, B_0 is taken in the y direction.

The following outline of the equations that govern the boundary layer is based on the aforementioned assumptions[22]:

$$\frac{\partial u}{\partial x} + \frac{\partial v}{\partial y} = 0 \tag{1}$$

$$u\frac{\partial u}{\partial x} + v\frac{\partial u}{\partial y} = \mu\left(1 + \frac{1}{\beta}\right)\frac{\partial^2 u}{\partial y^2} + \frac{3\mu(n-1)}{2}\Gamma^2\left(\frac{\partial u}{\partial y}\right)^2\frac{\partial^2 u}{\partial y^2} - \frac{\sigma B_x^2}{p_f}u \tag{2}$$

$$u\frac{\partial T}{\partial x} + v\frac{\partial T}{\partial y} = \alpha\frac{\partial^2 T}{\partial y^2} + \tau\left(D_B\frac{\partial C}{\partial y}.\frac{\partial T}{\partial y} + \frac{D_T}{T_\infty}\left(\frac{\partial T}{\partial y}\right)^2\right) \tag{3}$$

$$u\frac{\partial C}{\partial x} + v\frac{\partial C}{\partial y} = D_B\frac{\partial^2 C}{\partial y^2} + \left(\frac{D_T}{T_\infty}\right)\frac{\partial^2 T}{\partial y^2} \tag{4}$$

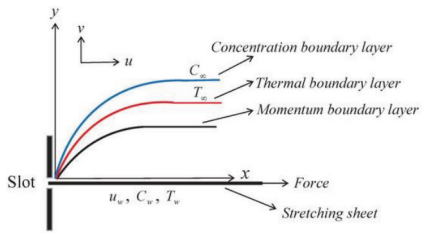


Figure 1. Geometrical representation.

Here u, v represents the velocity components in the x, y directions respectively, ρ_f - fluid flow density, ν - kinematic viscosity, $k^* = k_0 e^{-\frac{Nx}{L}}$ represent the permeability, k_0 is constant which gives initial permeability, σ -electric conductivity, τ - material constant, $(\rho C)_f$ - heat capacity, c -fluids concentration, $(\rho C)_p$ - heat capacity with fixed pressure, $\tau = \frac{(\rho C)_p}{(\rho C)_f}$, $\alpha = \frac{\kappa}{\rho C_f}$ - thermal diffusivity, T - Temperature, T_∞ - ambient temperature , D_∞ - Brownian diffusion, β - Casson parameter, and D_T - thermophoresis diffusion. $B(x) = B_0 e^{\frac{Nx}{2L}}$, applied magnetic field where B_0 being constant.

Subjected boundary conditions are:

$$\left.\begin{aligned} &u = U,\ v = 0,\ -\kappa\frac{\partial T}{\partial y} = h_f\left(T_f - T\right) \\ &D_B\frac{\partial c}{\partial y} + \frac{D_T}{T_\infty}\frac{\partial T}{\partial y} = 0 \ \text{ at } \ y = 0 \\ &u \to 0,\ v \to 0,\ T = T_\infty,\ c = c_\infty \ \text{ as } \ y \to \infty \end{aligned}\right\} \tag{5}$$

The classification of the similarity transformations is:

$$\begin{aligned} &U = U_w = Ue^{N_x/L} f'(\eta), V = -\sqrt{\frac{\vartheta U}{2L}} e^{N_x/2L} \\ &\left\{f(\eta) + \eta f^{'(\eta)}\right\}, \eta = y\sqrt{\frac{U}{2\vartheta L}} e^{N_x/2L} \end{aligned} \tag{6}$$

Equation (1), which is automatically fulfilled, using (6), (2-4) then converted to

$$\left(1 + \frac{1}{\beta}\right) f''' + N\left(ff'' - 2f'^2\right) + \frac{3(n-1)W_e}{2} f''f''' - Mf' = 0 \tag{7}$$

$$\begin{aligned} &(1+R)\theta'' + Pr\,N\left(f\theta' - f'\theta\right) + Nb\,\theta'\phi' + Nt\theta'^2 \\ &+ Ec\,Pr\frac{f''^2}{f'^2} - M\,\mathrm{Pr}\,Ec = 0 \end{aligned} \tag{8}$$

$$\phi'' + Sc\,N\left(f\phi' - f'\phi\right) + \frac{Nt}{Nb}\phi'' = 0 \tag{9}$$

with boundary conditions

$$\begin{aligned} &f(0) = 0,\ f'(0) = 1,\ \theta'(0) \\ &= -Bi\left(1 - \theta(0)\right),\ Nb\phi'(0) + Nt\,\theta'(0) = 0 \end{aligned} \tag{10}$$

$$f'(\eta) \to 0,\ \theta(\eta) \to 0,\ \phi(\eta) \to 0 \ as \ \eta \to \infty \tag{11}$$

Where $M = \frac{2\sigma B_0^2 L}{U_\rho}$ is magnetic parameter, $W_e = \frac{U^3 e^{3N_x/L}}{\vartheta L}$ Ã² is Weissenberg number, $Pr = \frac{\vartheta}{\alpha}$ is Prandtl number, $Nt = \frac{D_T\left(T_f - T_\infty\right)(\rho C)_p}{T_\infty\,\vartheta(\rho C)_f}$ is the thermophoresis parameter, $Nb = \frac{D_B\,C_\infty\,(\rho C)_p}{\vartheta(\rho C)_f}$ is the Brownian motion is parameter, $Sc = \frac{\vartheta}{D_B}$ is Schmidt number, $Ec = \frac{U_w^2}{(T_w - T_\infty)C_p}$ is Eckert number.

Nusselt number and drag coefficient are as follows

$$\sqrt{\frac{2}{R_e}} Nu_x = -\theta'(0), \tag{12}$$

$$\sqrt{R_e}\,Cf = \left(1 + \frac{1}{\beta}\right) f''(0) + \frac{(n-1)W_e^2}{2}\left(f'(0)\right)^3, \tag{13}$$

where local Reynolds number, $\mathrm{Re} = \frac{U_W L}{\nu}$.

3.0 Solution Procedure

The shooting technique is a numerical method used to solve Ordinary Differential Equations (ODEs) or boundary value problems by transforming them into initial value problems. It involves "shooting" an initial guess for the unknown variables and adjusting it iteratively until the desired boundary conditions are satisfied. Here's a basic overview of how the shooting technique works. If you have a boundary value problem, transform it into an initial value problem by guessing one boundary condition and treating the other as an unknown parameter. Make an initial guess for the unknown parameter(s) and solve the resulting initial value problem using a numerical ODE solver (e.g., Runge-Kutta methods) to obtain a solution. Compare the solution obtained from the initial value problem with the desired boundary condition

that you didn't use for the initial guess. Once the answer has been achieved fits the required boundary condition within a given tolerance, adjust the estimated parameter and continue steps repeatedly. You have discovered a numerical solution to the initial boundary value problem after the solution converges to the required boundary condition. The success of the shooting technique depends on the initial guess and the behavior of the solution. It's a trial-and-error process that requires careful adjustments and convergence monitoring.

4.0 Results and Discussion

The graph compares two types of non-Newtonian fluids: Casson fluid and Carreau fluid. Casson fluid is a model for shear-thinning fluids that have yield stress, which means they behave like a solid until a certain amount of force is applied. Carreau fluid is a model for fluids that have different viscosities at high and low shear rates, but no yield stress. Using the R-K-based shooting approach, the modified set of ODE's Eqs. (7)–(9), corresponding to Equestions (10) and (11) are resolved. We demonstrated how the magnetic field variable, the exponential variable, the Biot number, the thermophoresis variable, the Brownian momentum, and the value of the Weissenberg number affected the mass diffusion, velocity, and heating fields. In addition, we calculated the surface friction and Nusselt number.

Figure 2 shows how the dimensionless function $f(\eta)$ rises with the dimensionless parameter η for different values of the Weissenberg number W_e, which is a measure of how elastic a fluid is. The graph has three curves for $W_e = 1, 7$ and 10. The graph shows that both fluids have similar behavior at low values of η, but diverge at higher values. The Casson fluid has a lower value of $f(\eta)$ than the Carreau fluid for the same value of η, which means it has a lower viscosity. The Casson fluid also has a sharper drop in $f(\eta)$ as increases, which means it has a more pronounced shear-thinning effect.

Figure 3 shows that for both Casson and Carreau fluids, $\theta(\eta)$ decreases as η increases, meaning that the shear stress is lower near the wall of the pipe than at the center. This is because the fluid near the wall experiences a higher shear rate, which reduces its viscosity and makes it flow easier. The graph also shows that for both fluids, $\theta(\eta)$ decreases as We increases, meaning that the shear stress is lower for more elastic fluids. The graph also shows some differences between Casson and Carreau fluids. For Casson fluid, $\theta(\eta)$ has a minimum value at some intermediate value of η. This is because Casson fluid has a yield stress, which is a minimum amount of force needed to make it flow. Below this yield stress, Casson fluid behaves like a solid and does not deform. Above this yield

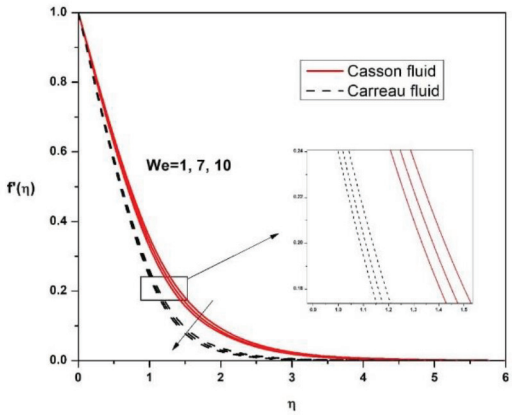


Figure 2. Effects of W_e on velocity fields.

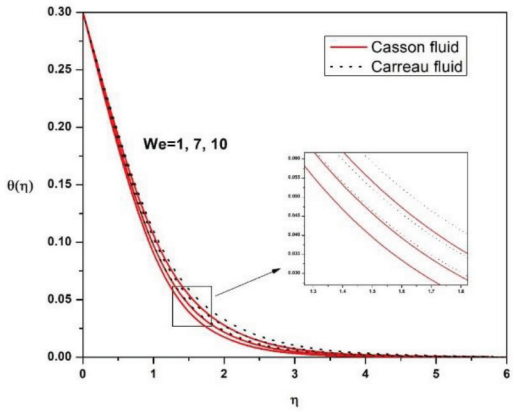


Figure 3. Effect of W_e on temperature fields.

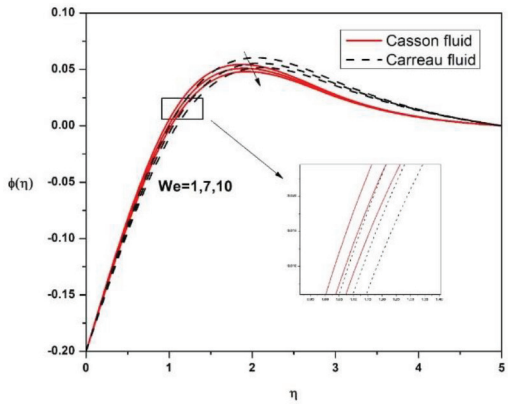


Figure 4. Effect of W_e on concentration fields.

stress, Casson fluid behaves like a power-law fluid, whose viscosity decreases with increasing shear rate. For Carreau fluid, $\theta(\eta)$ does not have a minimum value, but approaches a constant value as η approaches zero, meaning that there is no yield stress for Carreau fluid. Carreau fluid behaves like a Newtonian fluid at low and high shear rates.

Figure 4 shows the dimensionless shear stress $\phi(\eta)$, as a function of the dimensionless shear rate, for two different non-Newtonian fluid models: Casson and Carreau. The dimensionless quantities are obtained by dividing the actual shear stress and shear rate by some reference values.

The Carreau fluid model assumes that the fluid behaves like a Newtonian fluid at low and high shear rates, but has a variable viscosity at intermediate shear rates. The Carreau fluid model can also account for the shear-thinning behaviour of some fluids, which means that their viscosity decreases as the shear rate increases. The graph can be used to compare and contrast the behaviour of Casson and Carreau fluids under different flow conditions. For example, you can see that at low shear rates, both fluids have similar shear stresses, which means that they have similar viscosities. However, at high shear rates, the Casson fluid has a higher shear stress than the Carreau fluid which means that it has a higher viscosity. This implies that the Casson fluid is more resistant to flow than the Carreau fluid at high shear rates.

Figure 5 shows the velocity fields while M = 0.5, 2, 4. It is noticed that the velocity field decreases with increasing values of M, usually increasing the magnetic field produces the resistive force to the flow produced. The resistive force to the flow, such flow is known as Lorentz force $f(\eta) \to M$ dimensionless parameter that represents the ratio of the characteristic time to the residence time of the fluid in the pipe or channel. The graph shows that for both models, $\theta(\eta)$ increases as η increases, but at different rates. The Casson fluid curve is steeper than the Carreau fluid curve, which means that the Casson fluid has a higher viscosity than the Carreau fluid for the same value of η. The graph also shows that for both models, $f(\eta)$ approaches a constant value as η becomes very large, which means that both fluids behave like Newtonian fluids at high shear rates. However, the Casson fluid has a higher limiting value of $f(\eta)$ than the Carreau fluid, which means that it has a higher viscosity at infinite shear rate.

Figure 6 shows that both Casson and Carreau fluids have higher viscosity than Newtonian fluids at low shear rates, but lower viscosity than Newtonian fluids at high shear rates. The graph also shows that Casson fluid has a higher viscosity than Carreau fluid at low shear rates, but lower viscosity than Carreau fluid at high shear rates. The inset graph shows how the curves change for different values of M, which is a parameter related to the relaxation time of the fluid.

Figure 7 shows that both Casson fluid and Carreau fluid have lower shear stresses than Newtonian fluid (which has a constant viscosity) at low values of η, which means they flow more easily near the wall. However, as η increases, the shear stresses of both fluids increase faster than Newtonian fluid, which means they become more resistant to flow away from the wall. The graph also shows that Casson fluid has a higher shear stress than Carreau fluid at low values of η, but a lower shear stress than

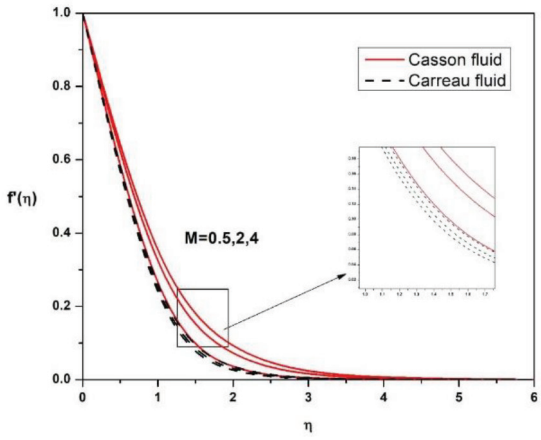


Figure 5. Consequences of M upon velocity.

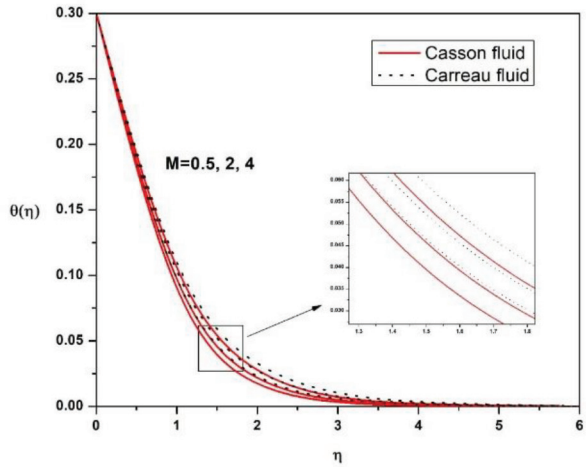


Figure 6. Effect of M on temperature fields.

Carreau fluid at high values of η . This means that Casson fluid has a higher yield stress but a lower viscosity than Carreau fluid. where both fluids have the same shear stress. This point corresponds to the value of η where the yield stress of Casson fluid equals the viscosity of Carreau fluid at zero shear rate.

Figure 8 shows the relationship between the dimensionless temperature $\theta(\eta)$ and the dimensionless distance η for two types of non-Newtonian fluids: Casson fluid and Carreau fluid. These fluids have different viscosity properties that depend on the shear rate. The graph also shows the effect of the Biot number Bi, which is a dimensionless parameter that measures the ratio of the internal and external thermal resistances of a body. From the graph, we can see that both fluids have similar trends of decreasing $\theta(\eta)$ with increasing η , which means that the temperature decreases as the distance from the surface increases. However, the Casson fluid has a steeper slope than the Carreau fluid, which implies that it has a higher heat transfer rate. We can also see that the Biot number affects the shape of the curves, where a higher Bi value leads to a more concave curve, while a lower Bi value leads to a more convex curve. This suggests that the Biot number influences the temperature gradient within the body, where a higher Bi value means a larger temperature difference between the surface and the interior, while a lower Bi value means a smaller temperature difference.

The Figure 9 shows how the dimensionless function $\phi(\eta)$ varies with the dimensionless parameter η for different values of Bi, which is a dimensionless number that represents the ratio of heat transfer due to convection and conduction. The graph compares the results for Casson fluid (solid red curve) and Carreau fluid (dashed black curve).

Figure 10 shows that both Casson and Carreau fluids have higher shear stress than Newtonian fluids at low shear rates, but lower shear stress than Newtonian fluids

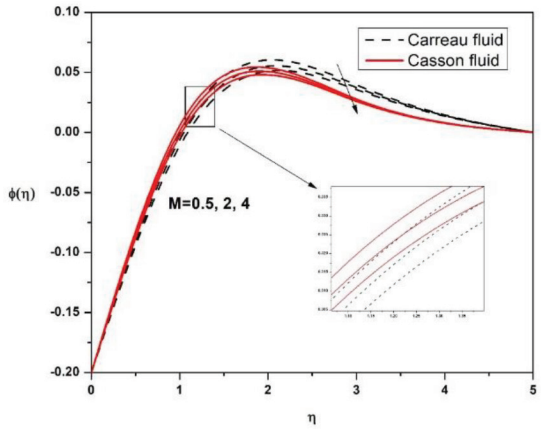


Figure 7. Effect of M on concentration fields.

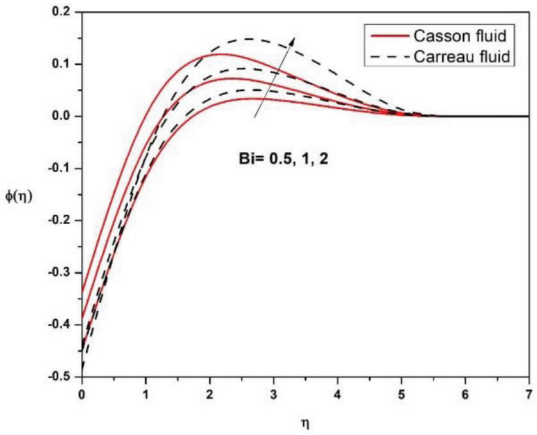


Figure 9. Effect of Bi on concentration fields.

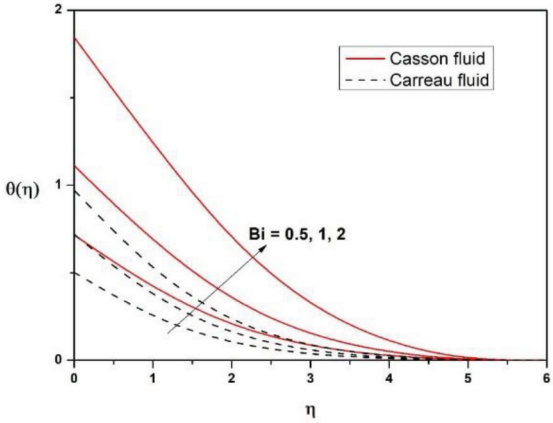


Figure 8. Effect of Bi on temperature fields.

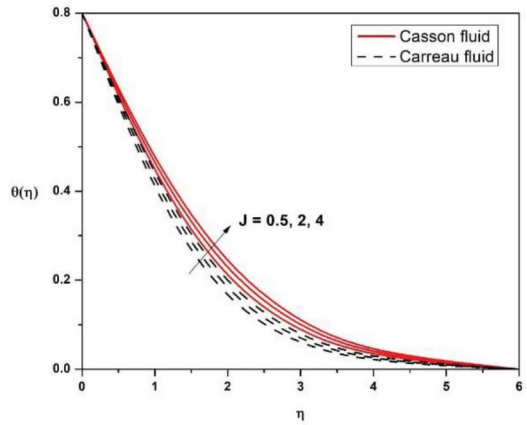


Figure 10. Effect of *J* on temperature fields.

at high shear rates. For different values of *J*, which is a dimensionless parameter that represents the ratio of viscous forces to elastic forces in the fluid. *J* = 0.5, 2, 4 are typical values for blood flow in arteries.

Figure 11 shows the relationship between a dimensionless parameter η and a function $\phi(\eta)$ for both Casson fluid and Carreau fluid. The parameter is related to the ratio of the wall shear stress to the yield stress for Casson fluid, and to the ratio of the wall shear rate to the relaxation time for Carreau fluid. The function $\phi(\eta)$ is related to the velocity profile of the fluid in a pipe. This parameter *j* is related to the ratio of the pressure gradient to the yield stress for Casson fluid, and to the ratio of the pressure gradient to the zero-shear viscosity for Carreau fluid. The graph shows that for both Casson fluid and Carreau fluid, $\phi(\eta)$ increases as η increases, but at different rates. The Casson fluid is smoother than the black Carreau fluid.

Figure 12 shows that for both models, $\theta(\eta)$ decreases as η increases, meaning that the viscosity decreases as the shear rate increases. However, the rate of decrease is different for each model and each value of η. For Casson fluid, $\theta(\eta)$ drops sharply from 1 to 0 as η increases from 0 to 1, meaning that there is a sudden change in viscosity at a critical shear rate. For Carreau fluid, $\theta(\eta)$ decreases gradually from 1 to 0 as η increases from 0 to infinity, meaning that there is a smooth transition in viscosity over a wide range of shear rates. The value of η affects how steep or flat the curve is: for higher values of n, $\theta(\eta)$ decreases more slowly, meaning that the viscosity is more sensitive to shear rate; for lower values of η, $\theta(\eta)$ decreases more quickly, meaning that the viscosity is less sensitive to shear rate.

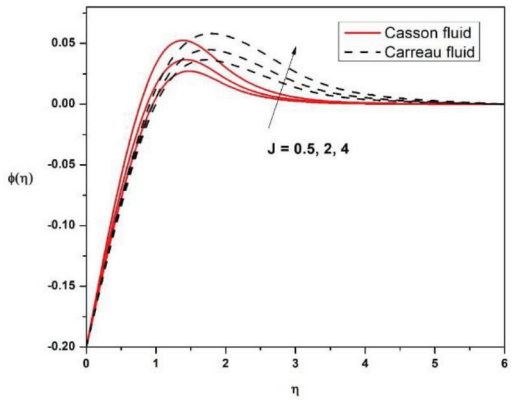


Figure 11. Effect of J on concentration fields.

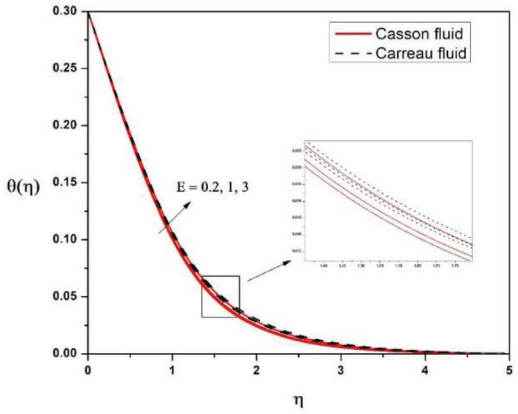


Figure 12. Effect of E_C on temperature fields

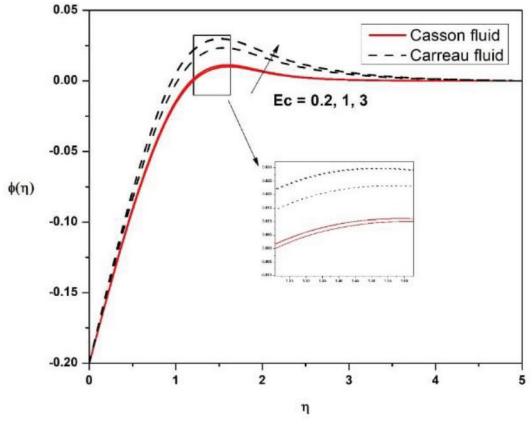


Figure 13. Effect of E_C on concentration fields.

Figure 13 shows how $\phi(\eta)$ varies with η for different values of E_C, which is the Eckert number. The Eckert number measures the effect of heat generation due to viscous dissipation. The inset graph shows that for Casson fluid, $\phi(\eta)$ increases as E_C increases, which means that heat generation increases the apparent viscosity and makes the fluid more resistant to flow. The graph also shows that Carreau fluid has a lower asymptotic value of $\phi(\eta)$ than Casson fluid, which means that Carreau fluid has a lower viscosity at high shear rates and flows more easily.

5.0 Conclusion

The temperature and concentration behaviour of Casson and Carreau fluids is investigated theoretically. For nanoparticles, passive management at their outermost layer is a more feasible scenario from a physical standpoint. Thus, we gave the Buongiorno model some

thought. The flow regulating equations are transformed into a dimensionless form by applying suitable similarity transformations. An efficient R-K-based shooting approach is then used to solve the altered equations. For most fluid instances, two alternatives are given. The following are the numerical results:

- Compared to Carreau fluid, Casson fluid has a somewhat greater thermal and mass transfer.
- Carreau and Casson fluids' heat transmission rates are both significantly increased by biot number.
- The parameters of thermophoresis and Brownian moment function similarly to those regulating concentration and temperature boundary layers.
- When compared to Casson fluid, the Lorentz force has a significant impact on the Carreau fluid.
- The exponential factor successfully increases the rate of transfer of heat of both fluids.
- The study sheds light on the migration of nanomaterials like metals, metal oxides, carbide particles, or carbon-based nanotubes.

6.0 References

1. Salah F, Almohammadi A. MHD boundary layer flow due to an exponentially stretching surface through porous medium with radiation effect. Int J Adv Appl Sci. 2023; 10(11):165-70. https://doi.org/10.21833/ijaas.2023.11.020
2. Senapati M, Parida SK, Swain K, Ibrahim SM. Analysis of variable magnetic field on chemically dissipative MHD boundary layer flow of Casson fluid over a nonlinearly stretching sheet with slip conditions. Int J Ambient Energy. 2022; 43(1):3712-26. https://doi.org/10.1080/01430750.2020.1831601
3. Seini YI, Makinde OD. MHD boundary layer flow due to exponential stretching surface with radiation and chemical reaction. Math Probl Eng. 2013; 2013:1-7. https://doi.org/10.1155/2013/163614
4. Alqahtani AM, Bilal M, Usman M, Alsenani TR, Ali A, Mahmuod SR. Heat and mass transfer through MHD Darcy Forchheimer Casson hybrid nanofluid flow across an exponential stretching sheet. ZAMM - J Appl Math Mech / Zeitschrift für Angew Math und Mech. 2023; 103(6): https://doi.org/10.1002/zamm.202200213
5. Eid MR. Chemical reaction effect on MHD boundary-layer flow of two-phase nanofluid model over an exponentially stretching sheet with a heat generation. J Mol Liq. 2016; 220:718-25. https://doi.org/10.1016/j.molliq.2016.05.005
6. Gireesha BJ, Kumar PBS, Mahanthesh B, Shehzad SA, Rauf A. Nonlinear 3D flow of Casson-Carreau fluids with homogeneous-heterogeneous reactions: A comparative study. Results Phys. 2017; 7:2762-70. https://doi.org/10.1016/j.rinp.2017.07.060
7. Nagendra N, Venkateswarlu B, Boulahia Z, Amanulla CH, Ramesh GK. Magneto Casson-Carreau fluid flow through a circular porous cylinder with partial slip. J Appl Comput Mech. 2022; 8(4):1208-21.
8. Raju CSK, Sandeep N. Unsteady three-dimensional flow of Casson-Carreau fluids past a stretching surface. Alexandria Eng J. 2016; 55(2):1115-26. https://doi.org/10.1016/j.aej.2016.03.023
9. Sobamowo G, Adesina OA, Jayesimi L. Magnetohydrodynamic flow of dissipative Casson-Carreau nanofluid over a stretching sheet embedded in a porous medium under the influence of thermal radiation and variable internal heat generation. Eng Appl Sci Lett. 2019; 2(2):18-36. https://doi.org/10.30538/psrp-easl2019.0018
10. Pramanik S. Casson fluid flow and heat transfer past an exponentially porous stretching surface in presence of thermal radiation. Ain Shams Eng J. 2014; 5(1):205-12. https://doi.org/10.1016/j.asej.2013.05.003
11. Hayat T, Shehzad SA, Alsaedi A. Soret and Dufour effects on magnetohydrodynamic (MHD) flow of Casson fluid. Appl Math Mech. 2012; 33(10):1301-12. https://doi.org/10.1007/s10483-012-1623-6
12. Sandeep N, Sulochana C. Dual solutions for unsteady mixed convection flow of MHD micropolar fluid over a stretching/shrinking sheet with non-uniform heat source/sink. Eng Sci Technol an Int J. 2015; 18(4):738-45. https://doi.org/10.1016/j.jestch.2015.05.006
13. Nadeem S, Ul Haq R, Lee C. MHD flow of a Casson fluid over an exponentially shrinking sheet. Sci Iran. 2012; 19(6):1550-3. https://doi.org/10.1016/j.scient.2012.10.021
14. Roopa KR, P. A. Dinesh, Yadav S, M. V. Govindaraju. Numerical technique for a Darcy-Forchheimer Casson CuO-MgO/methanol hybrid nanofluid flow due to an elongated curved surface with chemical reaction. J Mines, Met Fuels. 2023; 71(10):1431-41. https://doi.org/10.18311/jmmf/2023/35809
15. Amjad M, Khan MN, Ahmed K, Ahmed I, Akbar T, Eldin SM. Magnetohydrodynamics tangent hyperbolic nanofluid flow over an exponentially stretching sheet: Numerical investigation. Case Stud Therm Eng. 2023; 45:102900. https://doi.org/10.1016/j.csite.2023.102900
16. Bhattacharyya K, Layek GC. Magnetohydrodynamic Boundary layer flow of nanofluid over an exponentially stretching permeable sheet. Phys Res Int. 2014; 2014:1-12. https://doi.org/10.1155/2014/592536
17. Sharma S. MHD boundary layer flow past an exponentially stretching sheet with Darcy-Forchheimer flow of nanofluids. Indian J Sci Technol. 2022; 15(33):1594-604. https://doi.org/10.17485/IJST/v15i33.607

18. Mukhopadhyay S. MHD boundary layer flow and heat transfer over an exponentially stretching sheet embedded in a thermally stratified medium. Alexandria Eng J. 2013; 52(3):259-65. https://doi.org/10.1016/j.aej.2013.02.003
19. Mukhopadhyay S. Slip effects on MHD boundary layer flow over an exponentially stretching sheet with suction/blowing and thermal radiation. Ain Shams Eng J. 2013; 4(3):485-91. https://doi.org/10.1016/j.asej.2012.10.007
20. Khan U, Ahmed N, Asadullah M, Tauseef Mohyud-din S. Effects of viscous dissipation and slip velocity on two-dimensional and axisymmetric squeezing flow of Cu-water and Cu-kerosene nanofluids. Propuls Power Res. 2015; 4(1):40-9. https://doi.org/10.1016/j.jppr.2015.02.004
21. Yadav S, Dinesh PA, Roopa KR, Gogate SSP. Three-dimensional analysis of electromagnetic nano-material flow and thermal variations for forced convection. J Mines, Met Fuels. 2023; 71(10):1442-54. https://doi.org/10.18311/jmmf/2023/35810
22. Sathish Kumar M, Sandeep N, Rushi Kumar B, Dinesh PA., *et al*. A comparative analysis of magnetohydrodynamic non-Newtonian fluids flow over an exponential stretched sheet. Alexandria Eng J. 2018; 57(3):2093-100. https://doi.org/10.1016/j.aej.2017.06.002